Electronics and Electrical Engineering

http://www.aimspress.com/journal/ElectrEng

AIMS Electronics and Electrical Engineering, 6(4): 397–417.
DOI: 10.3934/electreng.2022024
Received: 23 August 2022
Revised: 09 October 2022
Accepted: 31 October 2022
Published: 04 November 2022

Research article

Smart deployment of energy storage and renewable energy sources for improving distribution system efficacy

Samarjit Patnaik[1,*], **Manas Ranjan Nayak**[1] **and Meera Viswavandya**[2]

[1] Department of Electrical Engineering, Biju Patnaik University of Technology, Rourkela 769015, Odisha, India

[2] Department of Electrical Engineering, Odisha University of Technology and Research, Bhubaneswar 751029, Odisha, India

* **Correspondence:** Email: patnaik.samarjit@gmail.com; Tel: +91-9438488168.

Abstract: Climate change, global warming, the depletion of fossil fuels, and rising energy demand are the main forces behind the increase in renewable energy sources. However, the unpredictability of power output from these renewable energy sources presents distribution system integration issues such as limited feeder capacity, unstable voltage, and network power loss. This study analyses the African vulture optimisation algorithm to determine the best allocation of distribution generators, with an emphasis on reducing the ageing of distribution transformers and delaying investment in feeders. The optimization technique provides faster global convergence and outperforms existing bio-inspired algorithms verified with benchmark uni-modal functions as a result of a larger crossover between the exploration and exploitation phases. The key aim is to decrease active power loss while simultaneously enhancing security margin and voltage stability. The IEEE 69-bus RDS system is utilised to validate the case studies for appropriate allocation of photovoltaic, wind turbine generation, and battery energy storage systems units, as well as offering the ideal energy management approach. During simulation, uncertainty on the characteristics of renewable energy source is accounted for. The results demonstrate the efficacy of the proposed algorithm with a substantial improvement in voltage profile, the benefit of lower CO2 emissions, an increase in security margin of up to 143%, and the advantage of extending the feeder investment deferral period by more than 50 years. In addition, the distribution transformer ageing acceleration factor improves significantly in the case of an increase in load demand.

Keywords: photovoltaic; distribution transformer ageing; battery energy storage system; wind turbine generation; African vulture optimisation; feeder investment deferral

Abbreviation

AVO	African vulture optimisation
BESS	Battery energy storage system
DE	Differential evolution optimisation
DG	Distributed generation
DISCOM	Distribution company
DT	Distribution transformer
FFA	Fire-fly algorithm
HST	Hot-spot temperature
MFO	Moth-flame optimisation
MINLP	Mixed-integer non-linear programming
NFL	No free lunch
PL	Power loss
VD	Voltage deviation
VS	Voltage stability
VSI	Voltage stability index
WTG	Wind turbine generation
PV	Photovoltaic
PSO	Particle swarm optimisation
RDS	Radial distribution system
RES	Renewable energy sources
RPPI	Renewable power production index
RTS	Residual tensile strength
SOC	State of charge

Nomenclature

P_{PV}	Output power of PV in kW
$P_{PV_{rated}}$	Rated power of PV module in kW
T_a	Ambient temperature in Celsius
η_P	Converter efficiency
I_c	Solar insolation
P_{WTG}	Output power of WTG in kW
$P_{WTG_{rated}}$	Rated power of WTG in kW
V_N	Nominal wind velocity
V_{cout}	Cut-out wind velocity
V_{cin}	Cut-in wind velocity
w_h	Load factor
C_i	Operating cost of i^{th} DG unit
γ_{VR}	Voltage regulation cost
γ_{loss}	Power loss cost
C_t	Electricity price at t^{th} hour
C_{Loss}	Cost of power loss
C_{VR}	Cost of voltage regulation
θ_{HST}	Hottest-spot winding temperature of DT in Celsius
θ_{TO}	Top oil temperature of DT in Celsius
F_t^{AA}	Accelerated ageing factor of DT
Lol_d	Percentage loss of life of DT
S_{T_x}	Power rating of DT
$T_{x_{Cap}}$	Installation cost of DT

1. Introduction

Nowadays, increased demands make radial distribution system (RDS) vulnerable to voltage drops and line losses. The distribution companies (DISCOM) are always aiming to expand to satisfy rising load requirements [1]. Building a new substation or enlarging the old one is the conventional solution to this problem. However, this is not economically sustainable due to the incurred operational expenses. Additionally, this technology has a detrimental influence on the environment due to its reliance on fossil fuels for electricity production. Utilizing photovoltaic (PV) solar energy, wind turbine generation (WTG), and several other distributed generators (DG) in distribution networks is a realistic option for reducing fossil fuel usage and achieving the United Nations sustainable development plan for climate change mitigation [2]. The objective of energy management using DGs of appropriate placement and size can be achieved. Recently published research has used numerous optimization techniques to tackle optimum DG allocation issues in radial distribution systems (RDS). The goals include the elimination of power loss (PL), the reduction of voltage deviation (VD), the maximisation of the voltage stability index (VSI), the enhancement of transient stability, the improvement of dependability, and the reduction of greenhouse gas emissions [3–5]. Incorporating BESS and DGs into the RDS improves the voltage profile of the lines. BESS often provides both technological and economic benefits [6].

The unpredictability of energy consumption raises the difficulty of occasionally overloading distribution transformers (DT) [7]. Sarker et al. [8] introduced an efficient charging technique that minimises the influence of load fluctuation on the ageing of a DT. A peak-shaving approach that increases the durability of DT insulation was formulated. Islam et al. [9] found that transferring loads to off-peak hours via an appropriate BESS management technique might extend the life of DTs. On the other hand, off-peak pricing might result in a new peak load during the early off-peak hours. Therefore, limiting DT life loss under higher load circumstances is necessary [10]. Setting maximum limitations on the DT to avoid overloads may seem to be a simple solution to the accelerated-ageing issue, given that transformer ageing is a function of its loading. However, such a strategy might overlook crucial loads at peak demand. Moreover, the authors have emphasised the utility's necessity for BESS charge management during off-peak hours. A substantial incentive has been recognised as cost minimization pricing. Frequently, the meta-heuristic algorithm may be separated into following categories: evolutionary algorithm, swarm intelligence, and physical algorithm. The meta-heuristics optimization approach primarily focuses on organism performance and accumulates the collective knowledge of all individuals. Meta-heuristic algorithms based on evolution are crucial to the theory of evolution for organisms. Meta-heuristic procedures based on a physical model are distinguished by whether search agent contact is signaled per the physical procedure's requirements. Although several solutions have been created, none can handle all optimisation difficulties. The No Free Lunch (NFL) argument reasonably shows the same [11]. This work presented the African vulture optimisation (AVO) algorithm, a population-based algorithm inspired by the lifestyle, food-seeking, and competition for food of various vultures. This method has a low computing cost and is more flexible than previous meta-heuristic algorithms; this is the proposed algorithm's defining characteristic and strength in balancing resonance and variability [12]. Comparing the suggested issues and proposed meta-heuristic algorithm to other robust meta-heuristic algorithms such as Particle Swarm Optimisation (PSO), Differential Evolution (DE), Moth-Flame Optimisation (MFO), Fire-Fly

algorithm (FFA), etc., it was discovered that the proposed meta-heuristic algorithm is exceptionally promising and superior compared to the current algorithms. However, with reference to computational complexity and execution time, this method is far more efficient compared to other similar algorithms, and it performs wonderfully when applied to large-scale problems.

From an objective standpoint, the capitalization of DG and BESS integration is seen as a multifaceted challenge. Several analytical approaches based on an precise formula have been utilised to address optimal DG integration issues [13], including mixed-integer nonlinear programming (MINLP), loss sensitivity, and others [14]. In the first step of the two-stage architecture described in [15], bus locations were identified based on voltage stability (VS) and loss sensitivity factors. The second step determined the optimal DG size using an analytical approach. Analytical procedures are user-friendly and require minimal processing time [16]. However, the aforementioned solutions are susceptible to various difficulties, including DG kinds, different DG unit numbers, and multi-objective functions [17]. The categorization of single and multi-objective optimization techniques is used to handle the DG allocation issues. The grid-connected PV and BESS optimise capacity and placement using an evolutionary algorithm. The best solution to a dual-objective optimisation issue is presented in as DG and BESS energy optimisation [18]. However, the transformer ageing factor for the distribution system under investigation was not established. In addition, none of the reviewed literature took into account the loss of energy energy, reliability, environmental benefits and operational consumer benefits of time-of-use pricing strategy in BESS, when they shift their charging profile that promotes the slowing of transformer ageing in a distribution system.

In order to fill the gap in previous research works, this paper proposes a multi-objective design for PV, WTG, and BESS systems that integrates technical, environmental, and economic goals using an interdisciplinary approach including the transformer loss of life cost. BESS management using time-of use pricing helps reduce peak load demand and improves DT ageing profile during increased load demand. PV and WTG help the environment by lowering greenhouse gas emissions from fossil fuel alternatives. The following summarises the primary contributions of this manuscript:

(1) The objective function is formulated, considering the advantages of reduction in voltage deviation index, benefit of reduction in environmental emission, distribution transformer ageing cost, and energy loss cost.

(2) A unique African vulture optimisation (AVO) technique is introduced to resolve highly nonlinear power system problems successfully.

(3) After integrating PV, WTG, and BESS, the system's performance in terms of voltage profile, security margin, energy loss, etc., has been evaluated.

(4) BESS's charging and discharging profiles have been analysed in light of time-of-use pricing.

(5) The improvement in feeder investment deferral time is analysed in light of the combination of DG and BESS.

(6) The ageing factor of distribution transformers is examined as the load demand increases.

The remainder of the paper is organised as follows. Section 2 of the paper focuses on modelling for PV, WTG, BESS, and load demand. The third section demonstrates the formulation of goal functions, system restrictions, and system parameters. Section 4 covers the principles of the African vulture algorithm, flowchart, and formulation. In Section 5, algorithm performance is evaluated using IEEE-69 bus RDS in various scenarios, and the results are compared and analysed. In the concluding portion of the study, the findings are summarised.

2. Modelling of system

The solar PV and BESS provide DC output, and WTG provides AC output power. A separate DC/DC converter is used for both PV and BESS, and for WTG, an AC/DC converter is used. The PV and WTG converters are unidirectional, and for BESS, a bidirectional converter is deployed. A bidirectional inverter transforms the DC power generated by the PV, WTG, and BESS to AC power. The system under consideration is a IEEE-69 bus radial distribution system and the loads are connected to different bus location. The consumer daily load variations across 24 hours are considered for the study. The exchange of power for the system and the utility grid is through a distribution transformer or a substation transformer. The placement of PV, WTG, and BESS bus locations in the RDS are at independent locations for providing maximum benefit to the system. The battery converter works as a charge controller throughout the BESS's charging procedure. The system's fundamental topology is presented in Figure 1.

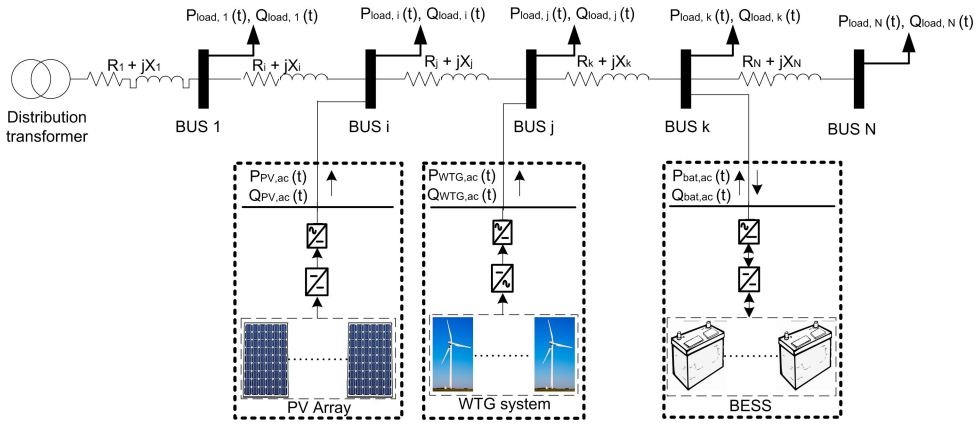

Figure 1. Single line diagram of RDS with PV, WTG and BESS.

2.1. Modelling of PV

The output power of photovoltaic systems is greatly influenced by the amount of sunlight they get. The solar irradiation profile [19] is shown as per Figure 2. Equation expresses the solar output power as can be evaluated as per (2.1).

$$P_{PV} = \eta_p P_{PV_{rated}} I_c (1 - 0.004(T_a - 25)) \tag{2.1}$$

where P_{PV} represents the PV output power (kW),T_a denotes the ambient temperature in degree celcius, I_c denotes the solar insolation on the PV module collector, $P_{PVrated}$ is the rated output power of the PV module, which is considered as 5 kW, and η_p is the converter efficiency including losses in the cable.

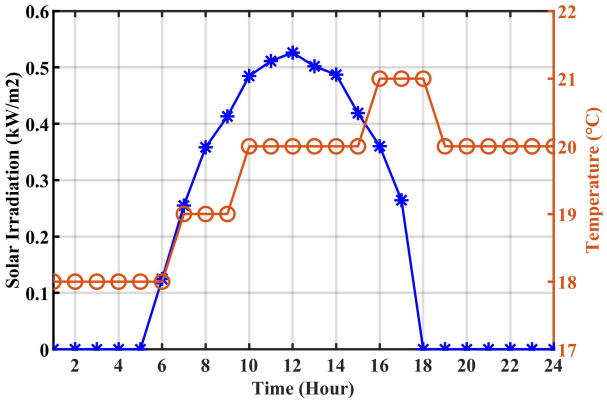

Figure 2. Solar insolation and ambient temperature.

2.2. Modelling of WTG

The mechanical power generation of WTG (P_{WTG}) depends on wind speed and can be evaluated using Eqn (2.2)

$$\begin{aligned} P_{WTG} &= 0 \quad , \quad V_{ag} < V_{cin} \;\; or \;\; V_{ag} > V_{cout} \\ &= (a * v_{ag}^3 + b * P_{WTG_{rated}}) \quad , \; V_{cin} \leq V_{ag} \leq V_N \\ &= P_{WTG_{rated}} \quad , \quad V_N \leq V_{ag} \leq V_{cout} \end{aligned} \tag{2.2}$$

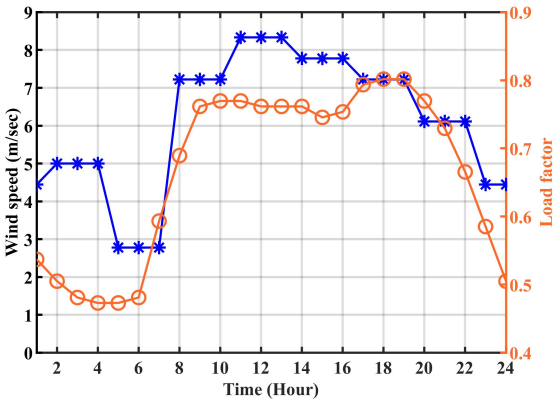

Figure 3. Load weight factor and wind speed.

$$\begin{aligned} a &= \frac{P_{WTG_{rated}}}{(V_N^3 - V_{cin}^3)} \\ b &= \frac{V_{cin}^3}{(V_N^3 - V_{cin}^3)} \end{aligned} \tag{2.3}$$

where $P_{WTG_{rated}} = 3\ kW$ represents the maximum amount of power that may be produced by WTG; (V_{cout}) represents the cut-out wind velocity. The wind speed variation for a typical day [20] is shown in

Figure 3. a and b are function of cut-in wind velocity (V_{cin}) and nominal wind velocity (V_N), and can be evaluated by Eqn (2.2) and Eqn (2.3).

2.3. Modelling of BESS

In this study, the BESS units are deployed at independent bus locations, which are not integrated with PV and WTG units. The BESS will support in peak shaving, and grid demand variation minimization. If excess power production is observed at the grid, the BESS is charged. In time t, the capacity or state of charge (SOC) $E_{k,t}$ of k^{th} BESS is updated [21] as Eqn (2.4) -

$$E^s_{k,t} = E^s_{k,t-1} + \mu_{k,t}\left(\sigma_{k,t-1} p^{ch}_{k,t} \eta^{ch}_k - \frac{(1-\sigma_{k,t})\, p^{dc}_{k,t}}{\eta^{dc}_k}\right) \tag{2.4}$$

where σ_k,h, $\mu_{k,t}$, $p^{ch}_{k,t}$, $p^{dc}_{k,t}$, η^{ch}_k and η^{dc}_k denotes the decision variables for charging, BESS participation, charging and discharging power, charging and discharging efficiencies, in time t of k^{th} BESS. The maximum obtainable charging capacities of a BESS, $UB^{ch}_{k,t}$, in time t along with charging decision variables are respectively evaluated as in Eqn (2.5) and Eqn (6) -

$$UB^{ch}_{k,t} = \begin{cases} 0, \quad \text{if } E^s_{k,t-1} = E^{Max}_k \\ P^{Max}_{ch,k} \quad \text{if } E^s_{k,t-1} + P^{Max}_{ch,k}\eta^{ch}_k \leqslant E^{Max}_k \\ \left(E^{Max}_k - E^s_{k,t-1}\right) \\ \quad \text{if } E^S_{k,t-1} + P^{Max}_{ch,k}\eta^{ch}_k > E^{Max}_k \end{cases} \tag{2.5}$$

$$\sigma_t = \begin{cases} 1 \quad \text{if} I^{SS}_t < 0 \\ 0 \quad \text{if} I^{SS}_t \geqslant 0 \end{cases} \quad \forall h \tag{2.6}$$

where E^{Max}_k, $P^{Max}_{ch,k}$, and I^{SS}_t represents the maximum capacity and maximum hourly power charging capacity of k^{th} BESS and, current injected from grid to RDS respectively. The BESS is typically discharged during peak demand hours to reduce power loss and voltage variation. The capacity $E_{k,t}$ will be adjusted as described in Eqn (2.4), however the maximum obtainable discharge limit of the BESS may be represented as Eqn (2.7) -

$$UB^{disch}_{k,t} = \begin{cases} 0, \quad \text{if} E^S_{k,t-1} \leqslant E^{Max}_k \\ -P^{Max}_{dc,k} \quad \text{if} E^S_{k,t-1} - \frac{P^{Max}_{dc,k}}{\eta^{dc}_k} \geqslant E^{Min}_k \\ -\left(E^S_{k,t-1} - E^{Min}_k\right) \\ \quad \text{if } E^S_{k,t-1} - \frac{P^{Max}_{dc,k}}{\eta^{dc}_k} < E^{Min}_k \end{cases} \tag{2.7}$$

Here, E^{Max}_k and $P^{Max}_{dc,k}$, are the BESS's minimum stated SOC and hourly power discharge limit.

2.4. Modelling of load

The IEEE 69-bus RDS system's load factor was calculated using test data collected across time periods of hours, days, weeks, and seasons and has been graphically shown in Figure 3. This Eq (2.8)

was used to estimate the real load demand for each bus, taking into consideration the bus's peak load demand. The projected load on bus i at any fixed instant t may be represented as follows:

$$P_{Load,j}(t) = w_h(t) \times P_j \tag{2.8}$$

where, $w_h(t)$ represents the load factor at instant t, P_j represents the load at the j^{th} node of the distribution system, and $P_{Load,j}(t)$ represents the load at instant t for the j^{th} node.

3. Problem formulation

The challenge entails determining the optimal position and size for PV, WTG, and BESS, as well as when they should be charged and discharged, while improving RDS's performance within the operational restrictions.

3.1. Objective function

The idea is to minimise distribution network power loss cost, DT aging cost, voltage regulation cost, operation cost of DGs and also improving renewable power production index. As a result, the mathematical formulation can be expressed as:

$$f_{obj} = min\left(\sum_{t=1}^{24}\left(\sum_{i=1}^{N}(C_i P_{DG_i}) + \sum_{j=1}^{B}\left(C_j P_{jt,dis}^{BESS}\right) - C_t P_{Gt} - \sum_{j=1}^{B}\left(C_j P_{jt,ch}^{BESS}\right)\right) + C_{VR} + C_{Loss} + C_{TxLol} - C_{ENV}\right) \tag{3.1}$$

where P_{DG_i} implies the output power from i^{th} DG unit, C_i implies the operating cost of i^{th} DG unit, C_j implies the operating cost of j^{th} BESS unit, $P_{jt,dis}^{BESS}$ is the BESS discharging power, $C_j P_{jt,ch}^{BESS}$ is the BESS charging power, P_{Gt} is the power received from grid, C_t is the electricity price at t^{th} hour, N represents number of DGs connected, B represents the number of battery storage units connected to the system, C_{VR} is the voltage regulation cost, C_{Loss} is the power loss cost, C_{TxLol} is the transformer aging cost and C_{ENV} is the environmental benefits of DGs [22–24].

$$C_{VR} = \left(\sum_{t=1}^{T}\sum_{i=1}^{N}\left(V_i - V_{ref}\right)\right) * \gamma_{VR} \tag{3.2}$$

$$C_{Loss} = \left(\sum_{t=1}^{T}\sum_{i=1}^{M}(Line\ Loss)\right) * \gamma_{Loss} \tag{3.3}$$

$$C_{ENV} = P_{DG} * RPPI \tag{3.4}$$

where N is the total bus number, V_i is the voltage at i^{th} bus (p.u.), V_{ref} is the reference voltage (1 p.u.), M is the branch number, γ_{VR} is the voltage regulation cost and γ_{loss} is the power loss cost ($\gamma_{VR} = 11.36\ Rs/p.u., \gamma_{loss} = 22.72\ Rs/kWh$) as per [25]. Adverse effects of pollutants emitted by fossil fuel power plants are the driving force for high penetration of renewable energy sources. The DGs have zero

emission and the savings on pollutant emissions have benefits. $RPPI = 1.2\ Rs/kWh$, is the renewable power production index representing the environmental benefits of DGs and the total economic benefits can be evaluated as per Eqn (3.4).

Insulation failure of a transformer may be analysed to determine the influence of DT ageing. The hottest-spot temperature (HST) of DT, that is the maximum temperature measured on the winding, is the primary cause of insulation breakdown. The technique for determining various temperatures, based on transformer loads and ambient temperature is outlined in IEEE standard C57.91.

$$\Theta^t_{HST} = \Theta^t_A + \Delta\Theta^t_{TO} + \Delta\Theta^t_{HST} \tag{3.5}$$

$$\Delta\Theta^t_{TO} = \Delta\Theta^{t-1}_{TO} + \left(\Delta\Theta_{TO,U} - \Delta\Theta^{t-1}_{TO,U}\right)\left(1 - e^{-\left(\frac{\Delta t}{\tau_{TO}}\right)}\right) \tag{3.6}$$

$$\Delta\Theta^t_{HST} = \Delta\Theta^{t-1}_{HST} + \left(\Delta\Theta_{HST,U} - \Delta\Theta^{t-1}_{HST,U}\right)\left(1 - e^{-\left(\frac{\Delta t}{\tau_w}\right)}\right) \tag{3.7}$$

$$\Delta\Theta^t_{TO,U} = \Delta\Theta^t_{TO,R}\left(\frac{k_t^2 R + 1}{R + 1}\right)^n \tag{3.8}$$

$$\Delta\Theta^t_{HST,U} = \Delta\Theta^t_{HST,R}\left(k_t^{2m}\right) \tag{3.9}$$

where Θ^t_A represents the ambient temperature, $\Delta\Theta^t_{TO}$ and $\Delta\Theta_{TO,U}$ represents the top-oil temperature increase and ultimate top-oil increase over the ambient conditions, $\Delta\Theta^t_{HST}$ represents the increase in winding HST over the top-oil temperature during the interval, $\Delta\Theta^t_{HST,U}$ represents ultimate HST increase over the top-oil temperature,$\Delta\Theta_{TO,R} = 55^0C$ represents the temperature increase of top-oil over ambient at standard load, $\Delta\Theta_{HST,R} = 25^0C$ represents the HST rise over top-oil at standard load, $\tau_{TO} = 5hr$ represents the top-oil time constant, $\tau_w = 0.2hr$ represents the winding time constant, k_t represents the ratio of the transformer load at time t to its rated capacity (4 MVA) , $R = 5.5$ is a factor of losses at rated load to no load, and $m = 0.8$ and $n = 0.8$ represents cooling parameters of the DT [17]. The value of $\Delta\Theta^t_{TO}$, $\Delta\Theta^t_{HST}$ can be calculated as per Eqn (3.6) and Eqn (3.7). The ultimate values of top-oil and HST increase can be evaluated using Eqn (3.8) and Eqn (3.9).

$$F^{AA}_t = e^{\left(\frac{15000}{110+273} - \frac{15000}{\theta^H_t + 273}\right)} \tag{3.10}$$

$$F_{eqa} = \sum_{t=1}^{T}\left(\frac{F^{AA}_t \Delta t}{T_d}\right) \tag{3.11}$$

$$Lol_d = \frac{F_{eqa} T_d * 100}{\beta} \tag{3.12}$$

$$C_{TxLol} = \frac{S_{Tx} T_{xCap} Lol_d}{100} \tag{3.13}$$

The DT ages more rapidly when its HST increases due to increased transformer loads. The accelerated ageing factor F_t^{AA} may be used to calculate the pace of ageing, which is a measure of how fast the insulation on a transformer breaks down in real life, in terms of deterioration under standard HST circumstances, which is chosen as 110^0C. Considering operation of DTs above this reference value, F^{AA} will exceed 1, indicating accelerated ageing. F^{AA} May be described as a function of exponential growth of Θ_{HST}, as given in Eqn (3.10). The value of F^{EQ} shows the comparable ageing (in days) of the transformer compared to the typical ageing as specified in Eqn 3.11, which is considered as 1 day for an oxygen-free, well-dried unit working at 110^0C. Lol_d represents the DT percent loss of life in hours while T_d is considered to be 24 hours and β denotes the standard insulation life of the DT. The oil-immersed transformer has an RTS of 20% at the reference temperature of 110^0C and a life expectancy of $150,000\ hr$ as its end-of-life criterion. The daily cost of transformer ageing may be computed using the formula in Eqn (3.12), where S_{Tx} and T_{xCap} are the transformer power rating of 4000 kVA and the transformer installation cost per unit of $1.2458 * 10^4\ Rs/kVA$, respectively.

3.2. System constraints

The system works within the confines of the following limits on equality and inequity -

$$P_{DT}(t) = P_{load}(t) + P_{loss}(t) - P_{PV}(t) - P_{WTG}(t) \mp P_{BESS}(t) \tag{3.14}$$

$$Q_{DT}(t) = Q_{load}(t) + Q_{loss}(t) - Q_{PV}(t) - Q_{WTG}(t) \mp Q_{BESS}(t) \tag{3.15}$$

$$SOC^{min} \leq SOC(t) \leq SOC^{max} \tag{3.16}$$

$$V_i^{min} \leq V_i(t) \leq V_i^{max} \tag{3.17}$$

$$I_{ij}(t) \leq I_{ij}^{max} \tag{3.18}$$

where $P_{DT}(t)$, $P_{load}(t)$, $P_{loss}(t)$, $P_{BESS}(t)$, $P_{PV}(t)$, $P_{WTG}(t)$, $Q_{DT}(t)$, $Q_{load}(t)$, $Q_{loss}(t)$, $Q_{BESS}(t)$, $Q_{PV}(t)$, represents power injected from distribution transformer, power supplied to load, transmission loss, BESS power injected to/received from grid , power generated from PV, power generated from WTG, reactive power injected from distribution transformer, reactive power supplied to load, reactive power loss, BESS reactive power injected/received from grid, reactive power generated from PV, reactive power generated from WTG respectively, at time t. SOC^{min} and SOC^{max} show the BESS's lowest and highest levels of charge.

3.3. System parameters

An IEEE 69-bus RDS system's branch current loading may be calculated utilising the security margin parameter. It is represented as a percentage of the rated branch current capacity as in Eqn (3.19).

$$min\left(\frac{I_{rated} - I_{actual}}{I_{rated}}\right) \tag{3.19}$$

Thermal stress damages a distribution system over time. Distribution feeders must be replaced or upgraded. The maximum thermal stress capacity is computed as (3.20).

$$S_{max} = S_a e^{ln\left(\frac{1+r_a}{100}\right)y} \tag{3.20}$$

where, S_a denotes the power requirement from grid at year $y = 0$, and r_a denotes the rise in load demand, which is assumed at 1.5 % per year.

4. African vulture optimisation (AVO) algorithm

This study is based on a novel meta-heuristic approach to vulture eating and seeking habits in Africa. Each of the African vultures has unique morphological characteristics, and the suggested algorithm consists of four distinct phases, each of which is detailed in detail below.

4.1. Identifying the two best vultures

The fitness of each solution is determined once the initial population has been generated. The optimum candidate is chosen as the best vulture in the first group, and the second-best candidate is chosen as the best vulture in the second group. Using Eqn (4.1), various solutions go near the best solutions for the first and second groups. The population is recalculated each time a fitness iteration is performed.

$$R(i) = \begin{cases} BestVulture_1 & if p_i = L_1 \\ BestVulture_2 & if p_i = L_2 \end{cases} \tag{4.1}$$

4.2. The rate of starvation of vultures

In good health, vultures can fly further in search of food, but when they are starving, they lack the endurance to keep up with the stronger vultures and, as a result, become aggressive toward the stronger vultures. To describe this behaviour mathematically, we used Eqn (4.2) as our starting point. In addition, it has been used to go from the exploration phase to the exploitation phase, which is based on the rate at which the vultures are either satiated or hungry. Quantifying the falling rate of satisfaction, Eqn (4.3) has been used to model this phenomenon.

$$t = h(sin^w\left(\frac{\pi}{2} * \frac{iteration_1}{maxiterations}\right) + cos\left(\frac{\pi}{2} * \frac{iteration_1}{maxiterations}\right) - 1) \tag{4.2}$$

$$F = (2 * rand_i + 1) * z * (1 - \frac{iteration_1}{maxiterations}) + t \tag{4.3}$$

4.3. Exploration

In the wild, vultures have excellent visual acuity and the capacity to identify food and recognise sick or dying animals. However, locating food for vultures may be quite challenging. In the AVO algorithm, vultures may scan various random regions depending on two distinct tactics, and a parameter known as P1 determines which approach to use. This option must be assigned a value between 0 and 1 before to the search operation, which determines which of the two search techniques is used.

$$P(i+1) = \begin{cases} R(i) - D(i) * F \geq rand_{p1} \\ R(i) - F + rand_2 * ((ub - lb) * rand_3 \\ +lb) < rand_{p1} \end{cases} \tag{4.4}$$

4.4. Exploitation

During this phase, the AVOA's efficiency stage is looked into. If F is below 1, the AVOA moves on to the exploitation phase. This phase also has two parts, and each part uses a different strategy. Two parameters, P2 and P3, show how likely it is that each strategy will be chosen in each internal phase. The first phase strategies are chosen with parameter P2, and the strategies available in the second phase are chosen with parameter P3. When the value of F is within 1 and 0.5, the AVOA enters the first phase of the Exploitation phase. In the first phase, there are two different flight and siege-fight strategies that are used in a rotating fashion. P2 is used to figure out which strategy each player will choose. This value must be between 0 and 1 before the searching operation is done. Eq (4.5) shows how to do this -

$$P(i+1) = \begin{cases} D(i) * (F + rand_4) - d(t) \geq rand_{p2} \\ R(i) - (S_1 + S_2) < rand_{p2} \end{cases} \tag{4.5}$$

$$S_1 = R(i) * \left(\frac{rand_5 * P(i)}{2\pi}\right) cos(P(i)) \tag{4.6}$$

$$S_2 = R(i) * \left(\frac{rand_6 * P(i)}{2\pi}\right) sin(P(i)) \tag{4.7}$$

Food Competition: When F = 0.5, the vultures are pretty full and have enough energy. When a lot of vultures gather around the same food source, it can lead to violent fights over the food. At these times, physically strong vultures don't like to share food with others. The weaker ones attempt to tire out the healthier ones and get food from them by gathering and engaging in little battles. This step is shown by Eqn (4.6) and (4.7).

$$D_i * (F + rand_4)\, sin(P(i)) \tag{4.8}$$

$$S_2 = R(i) * \left(\frac{rand_6 * P(i)}{2\pi} \right) sin(P(i)) \tag{4.9}$$

$$P(i+1) = R(i) - (S_1 + S_2) \tag{4.10}$$

In Eqn (4.9) and (4.10), R(i) indicates the location of the two optimum solutions, which is derived using Eqn (4.8). In Eqn (4.6) and (4.7), cos and sin correspond to the sine and cosine functions, respectively. The random numbers rand5 and rand6 are between 0 and 1. Finally, the location of the vultures is calculated using Eq (4.10).

We constructed our optimisation method in the manner described in Figure 4.

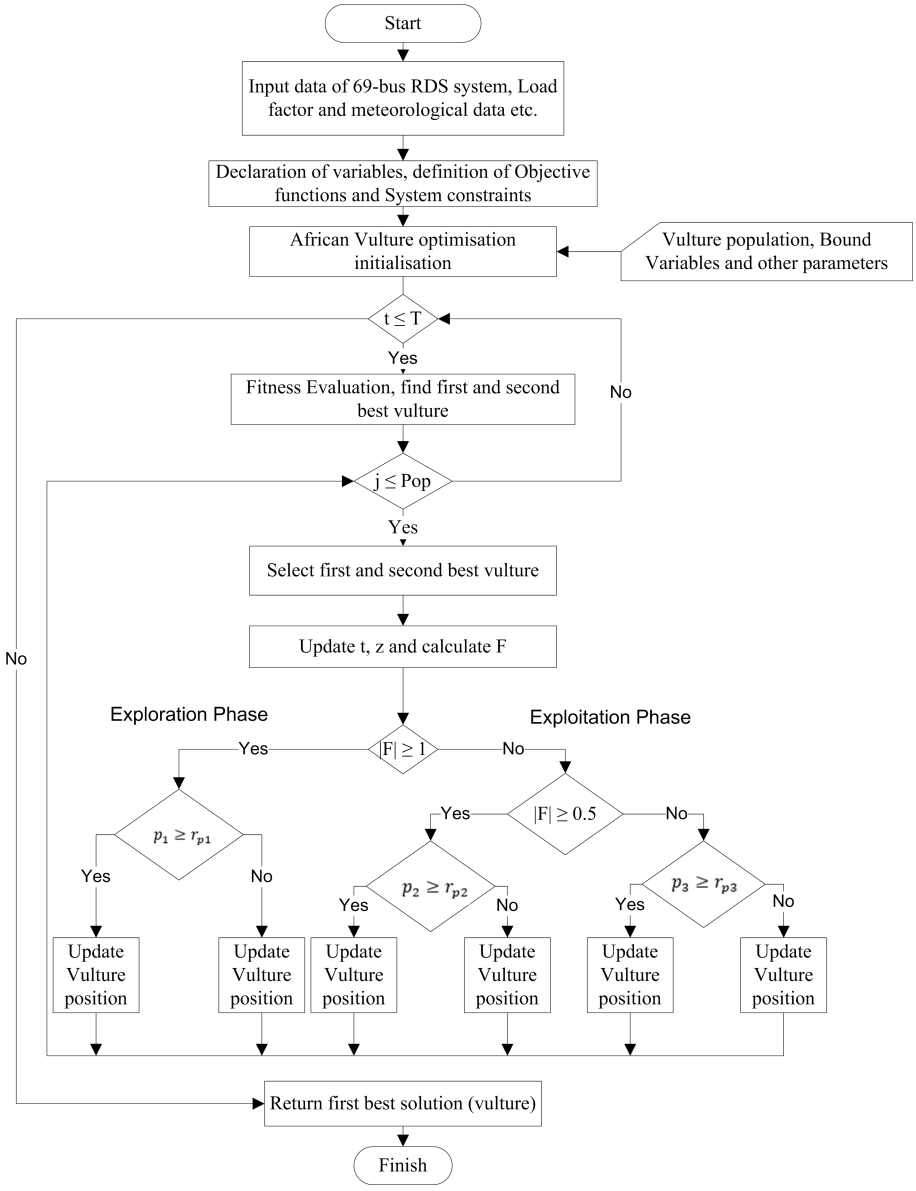

Figure 4. Flowchart of African vulture optimisation algorithm (AVOA).

4.5. Experiment and discussion

A series of simulation runs were conducted to compare the performance of the AVOA against that of other algorithms. There are six benchmark functions, including uni-modal and multi-modal functions, described in Table 1 for measuring the performance index.

Table 1. Benchmark functions.

Benchmark function type	Minimisation of function (Definition)	Range of variables
Uni-modal	$f_1(x) = \sum_{i=1}^{d} x_i^2$	$x = [-100, 100]$
Uni-modal	$f_2(x) = \sum_{i=1}^{d} \left(\sum_{j=1}^{d} x_j\right)^2$	$x \in [-100, 100]$
Uni-modal	$f_3(x) = \sum_{i=1}^{d-1} \left[100\left(x_{i+1} - x_i^2\right)^2 + (x_i - 1)^2\right]$	$x \in [-30, 30]$
Uni-modal	$f_4(x) = \sum_{i=1}^{d} (\lvert x_i + 0.5\rvert)^2$	$x \in [-100, 100]$
Multi-modal	$f_5(x) = -\sum_{i=1}^{d} \left(x_i Sin\left(\sqrt{\lvert x_i\rvert}\right)\right)^2$	$x \in [-500, 500]$
Multi-modal	$f_6(x) = -20exp\left(-0.2\sqrt{\frac{1}{d}\sum_{i=1}^{d} x_i^2}\right) - exp\left(\frac{1}{d}\sum_{i=1}^{d} cos2\pi x_i\right) + 20 + e$	$x \in [-32, 32]$

This performance evaluation of optimisation algorithm is based on the outcomes of 30 distinct runs containing 500 iterations. The standard deviation, mean error, worst error, and best error were determined and compared.

The performance metrics derived from MFO, FFA, PSO and DE algorithm and AVOA are compared in Table 2. As indicated in Table, AVOA has greatly outperformed other optimization methods while evaluating f1-f6 benchmark functions.

5. Results and analysis

The proposed method is evaluated by its implementation on IEEE 69-bus RDS. The AVO algorithm was used with the maximum population count of 50, number of iterations is 30 for all test cases. The backward-forward algorithm is used for solving load flow analysis. Valve regulated deep cycle lead acid Batteries having nominal voltage and current rating of 12 V and 97 Ah, respectively are used. The dispatch cycle of BESS is assumed in this research to be 24 hours long with an equal gap of one hour between each stage (s). Five distinct instances are analysed in the study are Case-1: Base case (without DG), Case-2: With PV only, Case-3: With WTG only, Case-4: With PV and WTG and Case-5: With PV, WTG and BESS.

The results obtained for each of the above cases are as below. The results indicate an improvement in reduction in power loss (Case-5) by 62% to 898.38 kW compared to base case (Case-1). The security margin of the system has also improved (Case-5) by 144% to 0.56 compared to 0.23 in base case (Case-1). The feeder deferal limit has been calculated by considering maximum apparent power demand in each cases throughout the day and base is taken as 4 MVA. Considering 5% increase in load in each year and maximum apparent power demand from grid in each cases, it was found that the feeder investment deferral will be maximum in Case-5 up to 55 $years$. This signifies the loads can be added to the existing RDS without additional investment in feeder expansion.

Table 2. Results of performance metric for benchmark funtion evaluation. (comparison with MFO, FFA, PSO and DE algorithms.

Benchmark function (Uni-modal / Multi-modal)	Parameter	AVOA	MFO	FFA	PSO	DE
$f_1(x)$ (Uni-modal)	Best	$5.44e-269$	$1.018e-01$	$2.27e-07$	$1.37e+03$	$7.46e-05$
	Worst	$6.05e-198$	$1.00e+04$	$2.17e-06$	$4.27e+03$	$7.89e-04$
	Mean	$2.01e-199$	$1.66e+03$	$7.88e-07$	$2.37e+03$	$3.36e-04$
	Std dev	$0.00e+00$	$4.36e-96$	$5.15e-07$	$6.17e-02$	$1.83e-04$
$f_2(x)$ (Uni-modal)	Best	$4.92e-217$	$3.45e+03$	$2.78e+03$	$4.07e+03$	$2.17e+04$
	Worst	$2.35e-142$	$4.49e+04$	$7.40e+03$	$2.29e+04$	$5.36e+04$
	Mean	$7.83e-145$	$2.23e+04$	$5.03e+03$	$9.20e+03$	$3.64e+04$
	Std dev	$4.29e-144$	$1.19e+04$	$1.32e+03$	$4.24e-03$	$7.01e+03$
$f_3(x)$ (Uni-modal)	Best	$1.96e-05$	$1.17e+02$	$1.51e+01$	$1.48e+05$	$2.75e+01$
	Worst	$2.56e-02$	$7.99e+07$	$1.85e+02$	$1.62e+06$	$2.38e+02$
	Mean	$6.50e-03$	$2.69e+06$	$7.31e+01$	$5.15e+05$	$6.00e+01$
	Std dev	$7.15e-03$	$1.45e+07$	$7.53e-01$	$3.37e-05$	$6.31e-01$
$f_4(x)$ (Uni-modal)	Best	$2.43e-07$	$2.80e-01$	$1.07e-06$	$1.19e+03$	$7.32e-05$
	Worst	$6.58e-06$	$1.95e+04$	$1.24e-01$	$3.55e+03$	$5.72e-04$
	Mean	$2.43e-06$	$2.66e+03$	$4.26e-03$	$2.35e+03$	$2.65e-04$
	Std dev	$1.89e-06$	$5.18e+03$	$2.25e-02$	$5.34e+02$	$1.47e-04$
$f_5(x)$ (Multi-modal)	Best	$-1.25e+04$	$-1.00e+04$	$-9.37e-03$	$-5.10e+03$	$7.32e-05$
	Worst	$-1.21e+04$	$-6.47e+03$	$4.88e+03$	$-2.69e+03$	$5.72e-04$
	Mean	$-1.25e+04$	$-8.51e+03$	$-6.89e+03$	$-3.82e+03$	$2.65e-04$
	Std dev	$1.00e+02$	$7.76e+02$	$1.14e+03$	$6.19e+02$	$1.47e-04$
$f_6(x)$ (Multi-modal)	Best	$8.89e-16$	$5.58e-01$	$9.24e-05$	$6.71e+00$	$3.04e-03$
	Worst	$8.89e-16$	$2.00e+01$	$8.73e-04$	$1.20e+01$	$7.78e-03$
	Mean	$8.89e-16$	$1.40e+01$	$3.44e-04$	$1.02e+01$	$5.19e-03$
	Std dev	$0.00e+00$	$7.67e-00$	$1.62e-04$	$1.30e-00$	$1.32e-03$

Table 3 summarises the findings for the suggested strategy for optimum size and positioning of PV, WTG and BESS.

Figure 5 indicates hourly minimum voltage profile for all test cases. It is observed that in Case-2 (PV only) the voltage profile improves from 6 AM to 6 PM considering the solar insolation during the period, however in Case-5 (PV, WTG and BESS) the system voltage profile improves throughout the day. Figure 6 represents the improvement in minimum hourly bus voltage profile in Case-5 as compared to other scenarios clearly across all nodes of RDS. Figure 7 indicates hourly minimum security margin profile for all test cases. It is observed that in Case-2 (PV only) the voltage profile improves from 6 AM to 6 PM, however in Case-5 (PV, WTG and BESS) the system security margin improves throughout the day. Figure 8 represents the improvement in minimum security margin profile in Case-5 as compared to other scenarios clearly across all branches of RDS.

Table 3. Results of the optimal solution for sizing & placement of PV, WTG and BESS.

Parameters	Base case	PV	WTG	PV & WTG	PV, WTG & BESS
Location of PV (Bus no)	-	53, 62, 69	-	24	8, 69
Size of PV (no of units)	-	124, 643, 176	-	39	77, 115
Location of WTG (Bus no)	-	-	9, 61, 69	2, 12, 62	21, 29, 61
Size of WTG (no of units)	-	-	183, 530, 246	34, 316, 528	115, 203, 430
Location of BESS (Bus no)	-	-	-	-	25, 69
Size of BESS (no of units)	-	-	-	-	500, 176
Total power loss (kW)	2346	1570.46	1007.84	983.63	898.38
Environmental cost benefit (Rs)	0	$3.6 * 10^4$	$5.37 * 10^4$	$5.43 * 10^4$	$5.45 * 10^4$
Min Sec Margin (per unit)	0.23	0.23	0.47	0.5	0.56
Min voltage (per unit)	0.929	0.929	0.953	0.955	0.957
Min Feeder deferral period (Yrs)	17	17	42	46	55

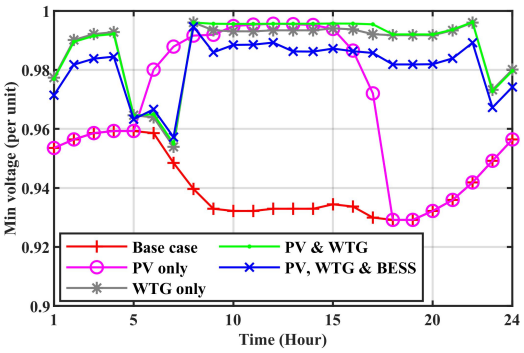

Figure 5. Hourly minimum bus voltage profile.

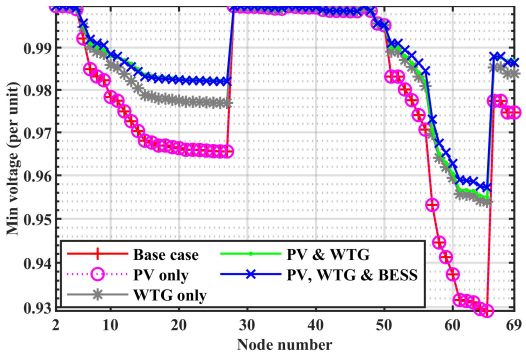

Figure 6. Minimum voltage of nodes in a day.

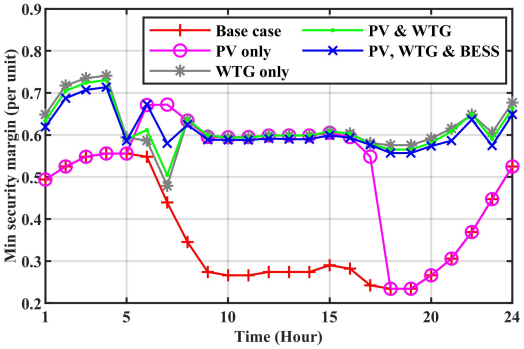

Figure 7. Hourly minimum security margin profile.

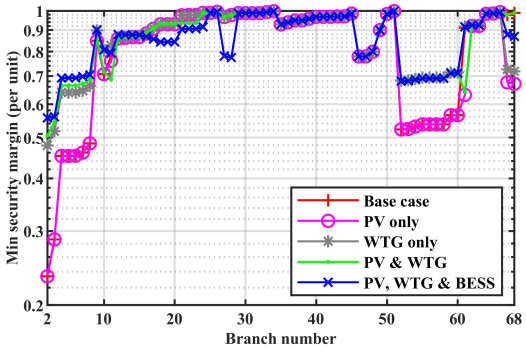

Figure 8. Minimum security margin in a day.

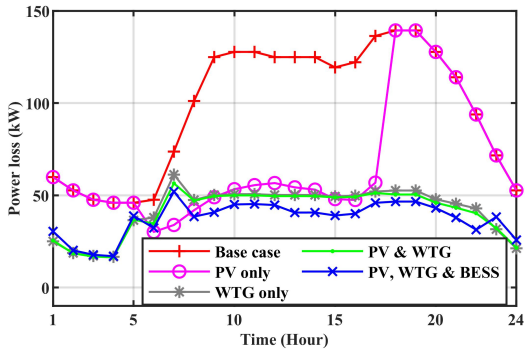

Figure 9. Hourly power loss profile.

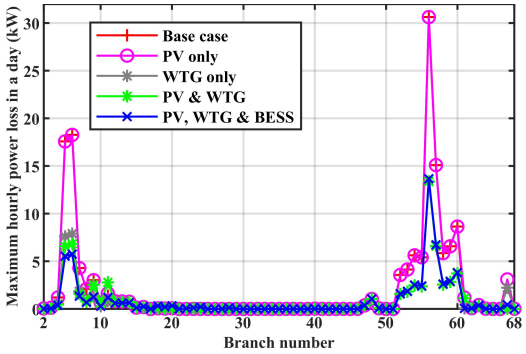

Figure 10. Minimum hourly power loss in a branch.

Figure 9 indicates hourly power loss profile for all test cases. It is observed that in Case-5 (PV, WTG and BESS) the hourly power loss is least throughout the day. Figure 10 represents the improvement in reduction in power loss profile in Case-5 as compared to other scenarios clearly across all branches of RDS. Figure 11 indicates the convergence curve of optimisation function with respect to iterations. The solutions converge for all cases and the minimum cost of objective function is achieved in Case-5. Figure 12 represents the state of charge after one cycle, which changes between the predefined lower and higher limits throughout a complete dispatch cycle of BESS. Figure 13 indicates the floating voltage of BESS and Figure 14 represents the current of BESS during charging and discharging cycle. Figure 15 indicates HST and DT aging acceleration factor profile. The five different cases were further compared with base load and an load increase of 50% of base load. It is clearly visible that the Case-1 has the highest HST and DT aging acceleration profile, which signifies the loss of life of DT. Whereas in Case-5 the HST profile and DT aging acceleration is minimum in both scenarios i.e., base load and in increased load condition as well. This will further improve the DT life and improve reliability of the system.

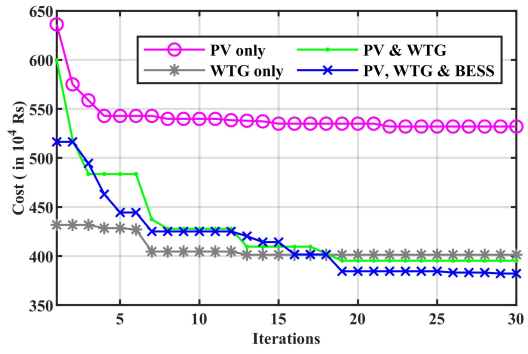

Figure 11. Optimisation Cost convergence.

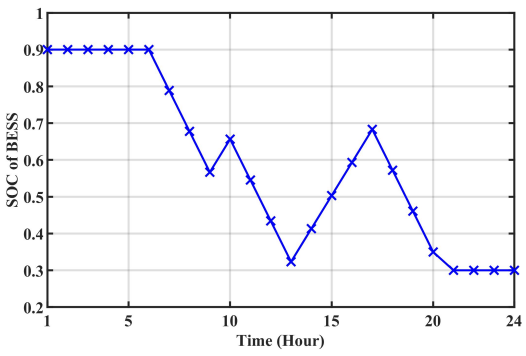

Figure 12. SOC of BESS.

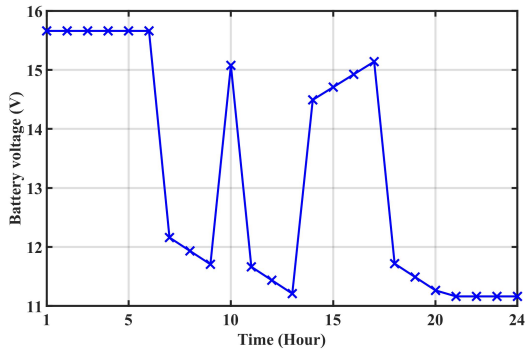

Figure 13. Voltage of BESS.

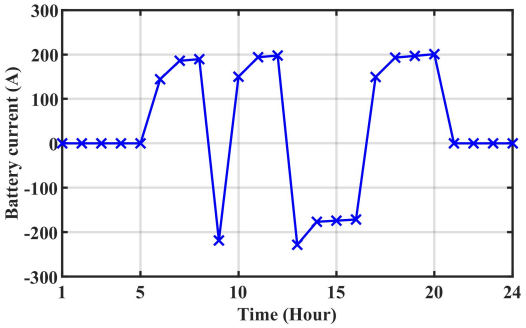

Figure 14. SOC of a dispatch cycle of BESS.

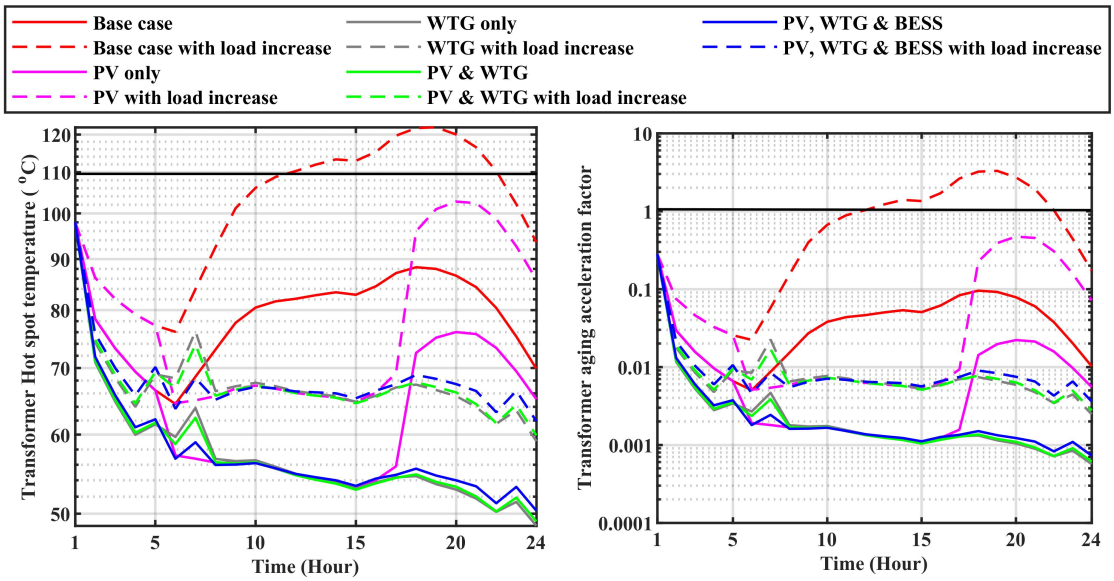

Figure 15. Status of HST and transformer aging acceleration factor of DT.

6. Conclusions

This work aims to optimally place and capacity planning of PV, WTG, and BESS in a radial distribution system using novel African Vulture optimisation (AVO) algorithm. The proposed work reduces transmission power loss with the optimal case having PV, WTG, and BESS simultaneous placement. There is an improvement in the increased minimum security margin of the system to 0.56 (per unit) from the base case value of 0.23 (per unit). Results indicate that the voltage profile of the system improves as well. Even in increased loading conditions, the transformer aging acceleration factors are significantly improved. The optimal scenario also attains peak saving, and peak demand from the grid during the 16^{th} to 20^{th} hour of the day is reduced, and thereby, the feeder capability is further enhanced. As a result, the investment for feeder expansion can be further deferred up to 55 years which is a significant economic benefit and benefits of reduction in equivalent savings on greenhouse gas emissions.Thus the proposed research shows inherent promise for improving

DT life span, increasing feeder investment deferral period, increased CO_2 savings with addition to improvement in system voltage, security margin and power loss. As a result, this research may be expanded to address additional complex multi-objective problems in a large-scale network.

Conflict of interest

The authors declare that there is no conflict of interest.

References

1. Akbar MI, Kazmi SAA, Alrumayh O, et al. (2022) A Novel Hybrid Optimization-Based Algorithm for the Single and Multi-Objective Achievement with Optimal DG Allocations in Distribution Networks. *IEEE Access* 10: 25669–25687. https://doi.org/10.1109/ACCESS.2022.3155484
2. Shaik MA, Mareddy PL, Visali N (2022) Enhancement of Voltage Profile in the Distribution system by Re-configuring with DG placement using Equilibrium Optimizer. *Alex Eng J* 61: 4081–4093. https://doi.org/10.1016/j.aej.2021.09.063
3. Ali A, Keerio MU, Laghari JA (2021) Optimal site and size of distributed generation allocation in radial distribution network using multi-objective optimization. *J Mod Power Syst Cle* 9: 404–415. https://doi.org/10.35833/MPCE.2019.000055
4. Hassan AS, Sun Y, Wang Z (2020) Multi-objective for optimal placement and sizing DG units in reducing loss of power and enhancing voltage profile using BPSO-SLFA. *Energy Rep* 77: 1581–1589. https://doi.org/10.1016/j.egyr.2020.06.013
5. Selim A, Kamel S, Jurado F (2020) Efficient optimization technique for multiple DG allocation in distribution networks. *Appl Soft Comput* 86: 105938. https://doi.org/10.1016/j.asoc.2019.105938
6. Sun Q, Huang B, Li D, et al. (2016) Optimal placement of energy storage devices in micro-grids via structure preserving energy function. *IEEE T Ind Inform* 12: 1166–1179. https://doi.org/10.1109/TII.2016.2557816
7. Visakh A, Selvan MP (2022) Smart charging of electric vehicles to minimize the cost of charging and the rate of transformer aging in a residential distribution network. *Turk J Electr Eng Co* 30: 927–942. https://doi.org/10.3906/elk-2106-80
8. Sarker MR, Olsen DJ, Ortega-Vazquez MA (2017) Co-Optimization of Distribution Transformer Aging and Energy Arbitrage Using Electric Vehicles. *IEEE T Smart Grid* 8: 2712–2722. https://doi.org/10.1109/TSG.2016.2535354
9. Islam JB, Rahman MT, Mokhlis H, et al. (2020) Combined analytic hierarchy process and binary particle swarm optimization for multi-objective plug-in electric vehicles charging coordination with time-of-use tariff. *Turk J Electr Eng Co* 28: 1314–1330. https://doi.org/10.3906/elk-1907-189
10. Qian K, Zhou C, Yuan Y (2015) Impacts of high penetration level of fully electric vehicles charging loads on the thermal ageing of power transformers. *Int J Elec Power* 65: 102–112. https://doi.org/10.1016/j.ijepes.2014.09.040
11. Adam SP, Alexandropoulos SAN, Pardalos PM, Vrahatis MN (2019) No free lunch theorem: A review. *Approximation and optimization* 145: 57–82. https://doi.org/10.1007/978-3-030-12767-1_5

12. Abdollahzadeh B, Gharehchopogh FS, Mirjalili S (2021) African vultures optimization algorithm: A new nature-inspired metaheuristic algorithm for global optimization problems. *Comput Ind Eng* 158: 107408. https://doi.org/10.1016/j.cie.2021.107408

13. Kasturi K, Nayak MR (2019) Assessment of techno-economic benefits for smart charging scheme of electric vehicles in residential distribution system. *Turk J Electr Eng Co* 27: 685–696. https://doi.org/10.3906/elk-1801-34

14. Montoya OD, Gil-González W, Rivas-Trujillo E (2020) Optimal Location-Reallocation of Battery Energy Storage Systems in DC Microgrids. *Energies* 13: 2289. https://doi.org/10.3390/en13092289

15. Azad S, Amiri MM, Heris MN, et al. (2021) A Novel Analytical Approach for Optimal Placement and Sizing of Distributed Generations in Radial Electrical Energy Distribution Systems. *Sustainability* 13: 10224. https://doi.org/10.3390/su131810224

16. Patnaik S, Nayak M, Viswavandya M (2022) Strategic integration of battery energy storage and photovoltaic at low voltage level considering multiobjective cost-benefit. *Turk J Electr Eng Co* 30: 1600–1620. https://doi.org/10.55730/1300-0632.3868

17. Sultana U, Khairuddin AB, Aman MM, et al. (2016) A review of optimum DG placement based on minimization of power losses and voltage stability enhancement of distribution system. *Renew Sust Energ Rev* 63: 363–378. https://doi.org/10.1016/j.rser.2016.05.056

18. Kumar A, Meena NK, Singh AR, et al. (2019) Strategic integration of battery energy storage systems with the provision of distributed ancillary services in active distribution systems. *Appl Energ* 253: 113503. https://doi.org/10.1016/j.apenergy.2019.113503

19. Patnaik S, Ray S, Kasturi K, et al. (2022) Optimal allocation of DGs for non-linear objective function modeling in a three-phase unbalanced distribution system using crow search optimization algorithm. *J Interdiscip Math* 25: 681–701. https://doi.org/10.1080/09720502.2021.2012894

20. Kasturi K, Nayak CK, Patnaik S, et al. (2022) Strategic integration of photovoltaic, battery energy storage and switchable capacitor for multi-objective optimization of low voltage electricity grid: Assessing grid benefits. *Renewable Energy Focus* 41: 104–117. https://doi.org/10.1016/j.ref.2022.02.006

21. Ahmed HM, Awad AS, Ahmed MH, et al. (2020) Mitigating voltage-sag and voltage-deviation problems in distribution networks using battery energy storage systems. *Electr Pow Syst Res* 184: 106294. https://doi.org/10.1016/j.epsr.2020.106294

22. Boonluk P, Siritaratiwat A, Fuangfoo P, Khunkitti S (2020) Optimal Siting and Sizing of Battery Energy Storage Systems for Distribution Network of Distribution System Operators. *Batteries* 6: 56. https://doi.org/10.3390/batteries6040056

23. Wang L, Singh C (2009) Multicriteria design of hybrid power generation systems based on a modified particle swarm optimization algorithm. *IEEE T Energy Conver* 24: 163–172. https://doi.org/10.1109/TEC.2008.2005280

24. Chedid R, Rahman S (1997) Unit sizing and control of hybrid wind-solar power systems. *IEEE T Energy Conver* 12: 79–85. https://doi.org/10.1109/60.577284

25. Srithapon C, Ghosh P, Siritaratiwat A, et al. (2020) Optimization of electric vehicle charging scheduling in urban village networks considering energy arbitrage and distribution cost. *Energies* 13: 349. https://doi.org/10.3390/en13020349

AIMS Press